

## Supporting Information

### Chemical Characterization of Localized Radicals in *closo*-Borate Anion Derivatives

Jaskiran Kaur,<sup>#a</sup> Markus Rohdenburg,<sup>#b</sup> Kirsten Zeitler,<sup>c</sup> Judy K. Y. Liu,<sup>a</sup> Carsten Jenne,<sup>d</sup> Maik Finze,<sup>e</sup> Hilikka I. Kenttämäa,<sup>a</sup> Jonas Warneke,<sup>b,f,\*</sup>

#### Table of Contents

S1 Mass spectra measured after ion-molecule reactions with dimethyl disulfide (DMDS) .....	2
S2 Mass spectra measured after ion-molecule reactions with methyl acrylate (MA).....	3
S3 Mass spectra measured after ion-molecule reactions with styrene (ST) .....	4
S4 Mass spectra measured after ion-molecule reactions with methyl acrylate (MA) and styrene (ST) ...	5
S5 Zoomed-in mass spectra measured after ion-molecule reactions of ion B with methyl acrylate (MA) and styrene (ST) .....	6
S6 Mass spectrum measured after ion-molecule reactions of ion 5 with methyl acrylate (MA) and styrene (ST) .....	6
S7 ESP-mapped calculated molecular surfaces of ions 1-5, Q, and B .....	7
S8 Methodological problems during assigning $\omega$ and $\omega^-$ to charged species in cDFT.....	7
S9 Mass spectrum measured after ion-molecule reactions of ions 1 and 2 with CCl <sub>4</sub> .....	9
S10 Relative abundances of the reactant and product ions as a function of time for the reactions of ions Q, B and 1-5 with allyl iodide .....	10
S11 Mass spectrum measured after ion-molecule reactions of ion 5 with allyl iodide .....	11
S12 Mass spectrum measured after ion-molecule reactions with allyl chloride .....	12
S13 PES comparison between borane radicals and phenyl/quinoline radicals .....	13
S14 PES for the reaction of allyl iodide with the hypothetical derivative [HCB <sub>11</sub> F <sub>10</sub> ] <sup>•</sup> .....	14
S15 Calculated geometries of CC(I), TS(I) and CA(I) for ions 1 and Q .....	14
S16 Energy decomposition analysis of TS(DB) for ions 3, 4 and B .....	15
S17 References.....	15

### S1 Mass spectra measured after ion-molecule reactions with dimethyl disulfide (DMS)

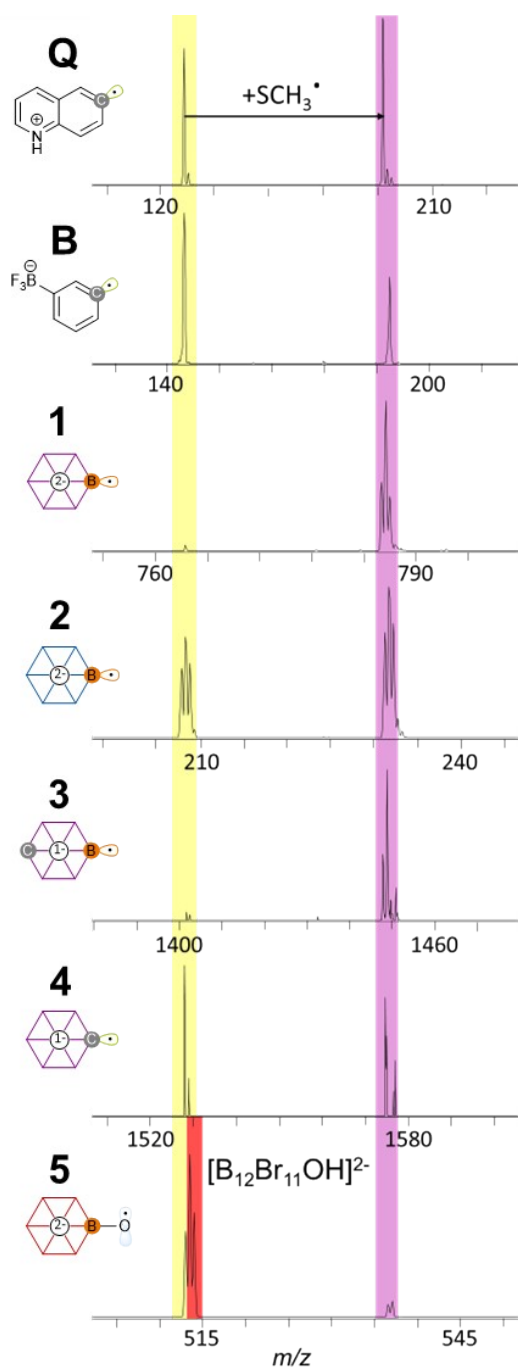


Figure S1: Mass spectra obtained after 30 ms reactions between isolated ions **Q**, **B** and **1-5** with dimethyl disulfide in the ion trap of a linear quadrupole ion trap mass spectrometer. The signal of the isolated radical ion is marked yellow. The signal of the product formed upon abstraction of  $[SCH_3]^\bullet$  is marked purple. In the case of ion **5**, H atom abstraction is the major reaction pathway and the product signal is marked in red.

**S2 Mass spectra measured after ion-molecule reactions with methyl acrylate (MA)**

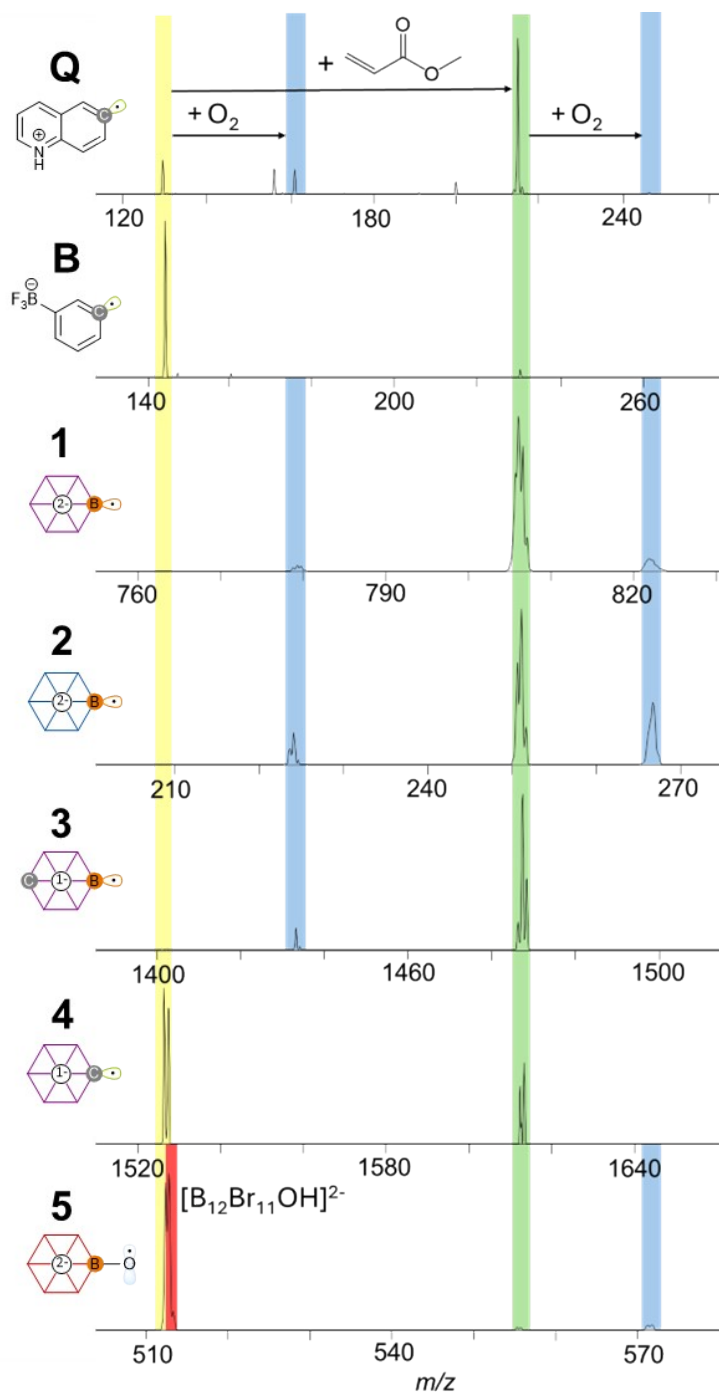


Figure S2; Mass spectra obtained after 1000 ms reactions between isolated ions **Q**, **B** and **1-4** with methyl acrylate and 3000 ms reactions between isolated ion **5** with methyl acrylate in the ion trap of a linear quadrupole ion trap mass spectrometer. The signal of the isolated radical ion is marked yellow. The signal of the stable adduct ions is marked green. In the case of ion **5**, H atom abstraction is the major reaction pathway, and the product signal is marked in red. Binding with residual  $O_2$  gas is marked in blue.

### S3 Mass spectra measured after ion-molecule reactions with styrene (ST)

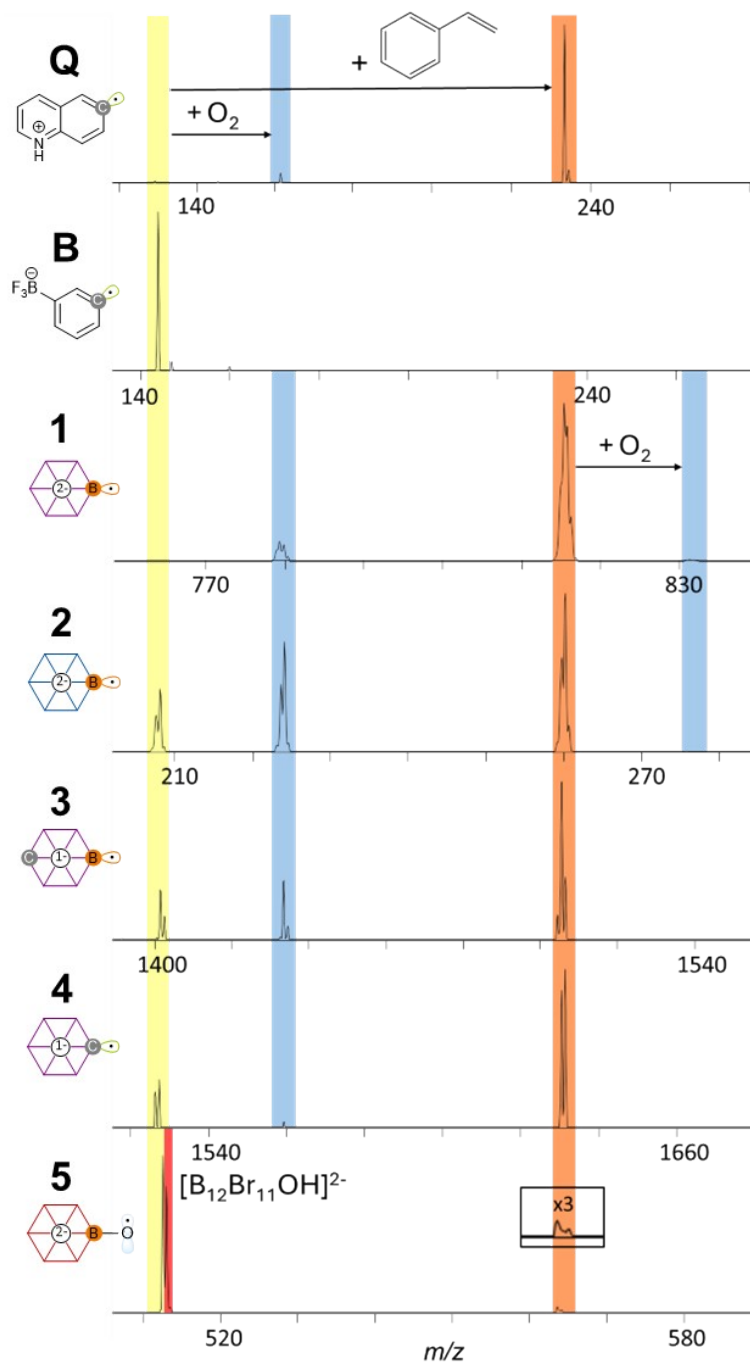


Figure S3: Mass spectra obtained after 1000 ms reactions between isolated ions **Q**, **B** and **1-4** with styrene and 3000 ms reactions between isolated ion **5** with styrene in the ion trap of a linear quadrupole ion trap mass spectrometer. The signal of the isolated radical ion is marked yellow. The signal of the stable adduct ions is marked orange. In the case of ion **5**, H atom abstraction is the major reaction pathway, and the product signal is marked in red. Binding with residual  $O_2$  gas is marked in blue.

S4 Mass spectra measured after ion-molecule reactions with methyl acrylate (MA) and styrene (ST)

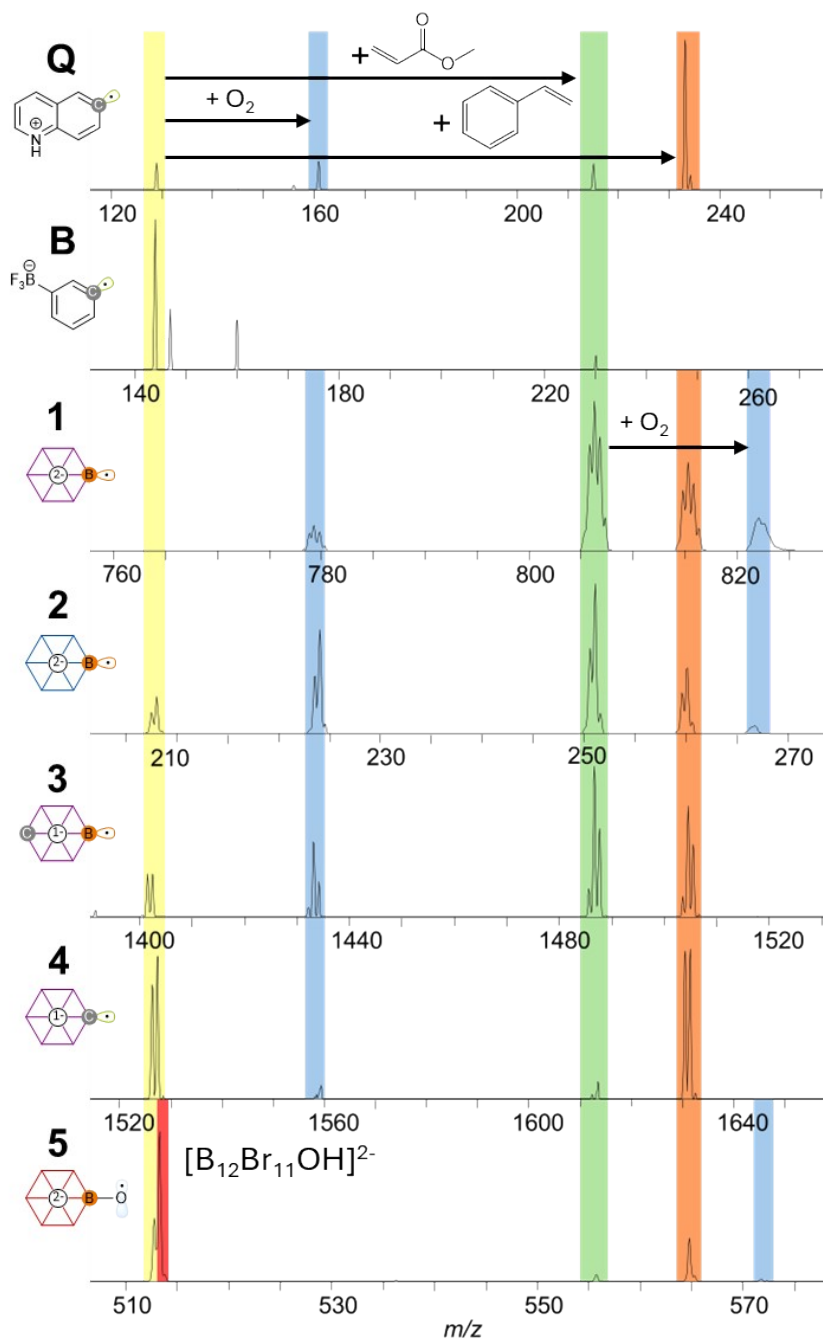


Figure S4: Mass spectra obtained after 1000 ms reactions between isolated ions **1-4**, **B**, and **Q** with a mixture of MA and ST and 3000 ms reactions between isolated ion (**5**) with a mixture of MA and ST in the ion trap of a linear quadrupole ion trap mass spectrometer. The signal of the isolated radical ion is marked yellow. The signal of the product received by MA binding is marked green and the signal obtained by ST binding is marked orange. In the case of ion **5**, H atom abstraction occurs as the major reaction pathway and the product signal is marked in red.

### S5 Zoomed-in mass spectra measured after ion-molecule reactions of ion B with methyl acrylate (MA) and styrene (ST)

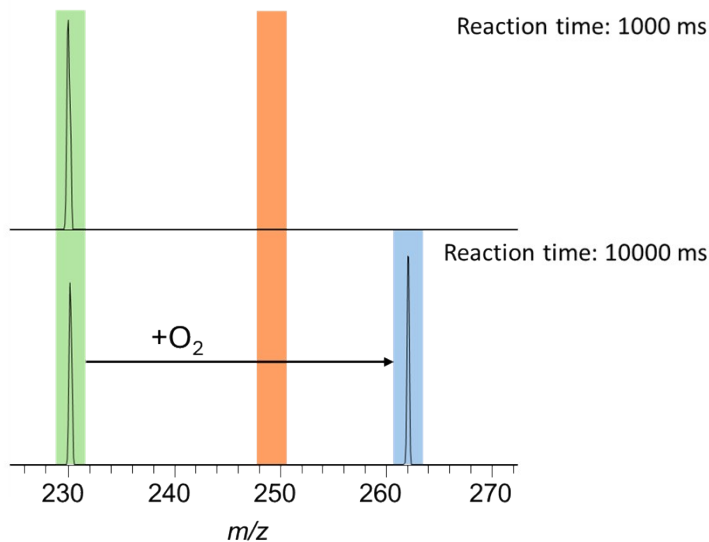


Figure S5: Section of ion-molecule reaction mass spectra obtained after 1000 ms (top) and 10000 ms (bottom) reactions of isolated ion **B** with MA and ST in the ion trap of a linear quadrupole ion trap mass spectrometer. Green marks the product formed by MA binding. Blue marks an ion formed by O<sub>2</sub> binding of the MA-product. Ion **B** does not react with ST (marked in orange).

### S6 Mass spectrum measured after ion-molecule reactions of ion 5 with methyl acrylate (MA) and styrene (ST)

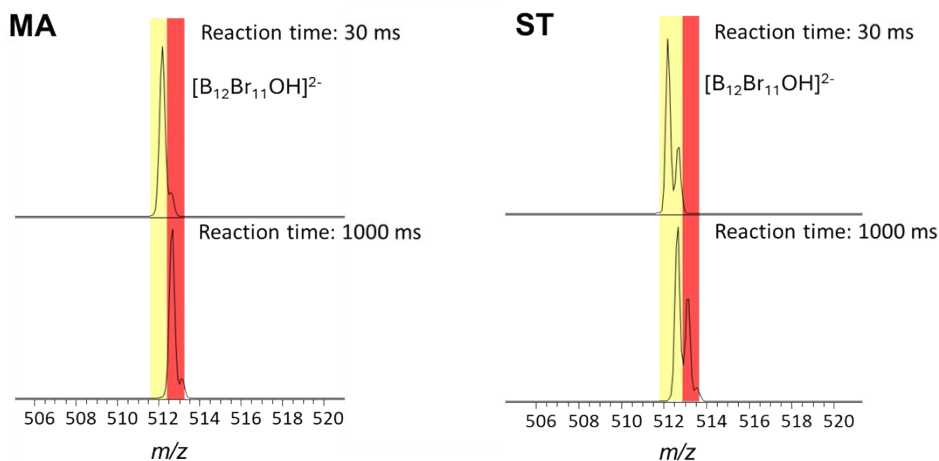


Figure S6: Section of ion-molecule reaction mass spectra obtained after 30 ms (top) and 1000 ms (bottom) reactions of isolated ion **5** with MA (left) and 30 ms (top) and 10000 ms (bottom) reactions of isolated ion **5** with ST (right) in the ion trap of a linear quadrupole ion trap mass spectrometer. The signal of the isolated radical ion is marked yellow. The H atom abstraction product is marked in red.

### S7 ESP-mapped calculated molecular surfaces of ions 1-5, Q, and B

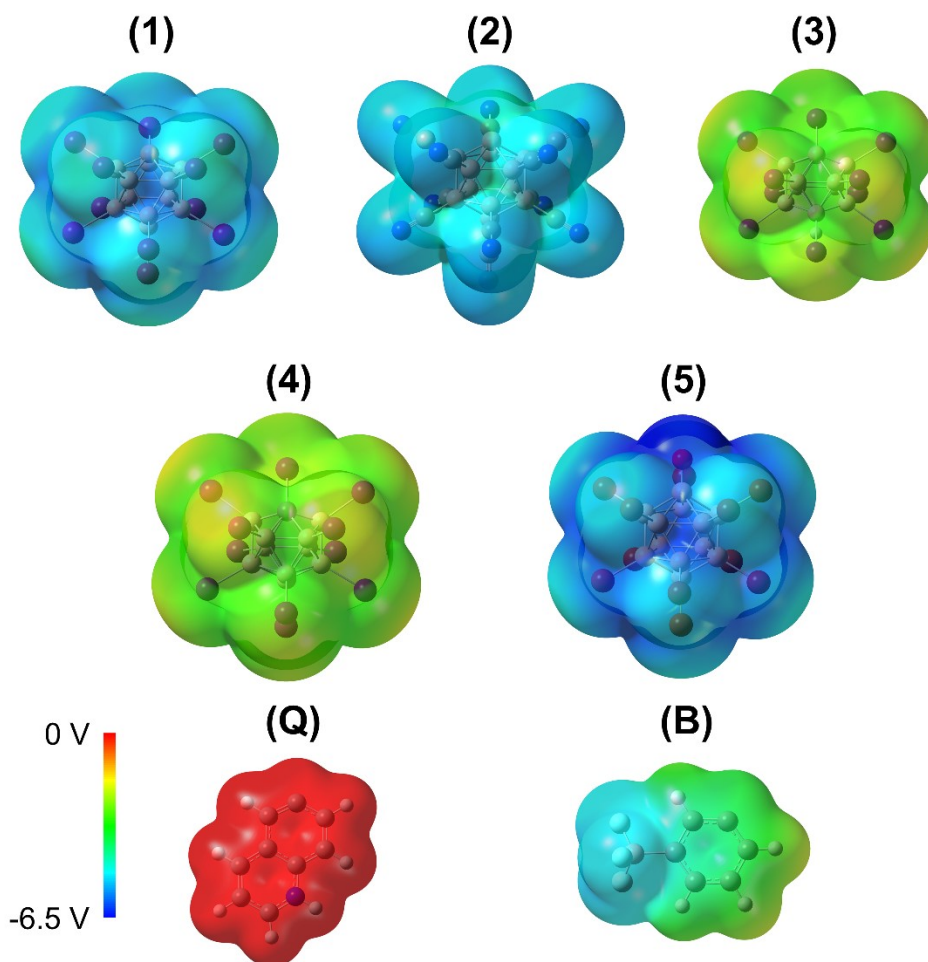


Figure S7: Calculated electrostatic potentials (ESP) mapped onto the molecular surfaces (0.001 a.u. electron density isosurfaces) of ions **1-5**, **Q**, and **B**, calculated on B3LYP-D3BJ/def2-TZVPP level. The color code including lower and upper limits (converted to V) is given in the bottom left corner.

### S8 Methodological problems during assigning $\omega$ and $\omega^*$ to charged species in cDFT

The electrophilicity index  $\omega$  used in numerous previous studies uses ionization potentials (IP) and electron affinities (EA), which describe the energy required to bring an electron from the radical to infinite distance, or the energy gained by the approach of an electron from infinite distance and its attachment to the radical, respectively. The sum of these quantities is used to calculate the chemical potential  $\mu$  and its inverse, the Pauling electronegativity  $\chi$ , and their difference is used to calculate the hardness  $\eta$ , both of which are eventually used to calculate  $\omega$  according to equation (S1).

$$\omega = \frac{\chi^2}{2\eta} = \frac{1}{8} \frac{(IE + EA)^2}{IE - EA} \quad (\text{S1})$$

This approach of describing electrophilicity is thus based on the assumption that the energetics of receiving electron density from a reagent correlates with the energetics of attaching an electron. Similarly,

it is assumed that the energetics of providing electron density to a reactant correlates with IP. These assumptions conceptually appear reasonable for neutral radicals, and as described several times in literature, have well predicted trends in radical selectivities towards electrophilic and nucleophilic reaction partners. However, we want to raise attention about issues with a direct transfer of this concept to ionic radicals: If a radical carries a non-zero charge, the energetics of electron attachment (value of EA) and electron detachment (value of IP) are largely determined by the long-range Coulomb interaction between two charges (ion & electron), whereas receiving or releasing of electron density for bond formation with a neutral reaction partner is not. The energy contribution of the long-range ion-electron interaction in the calculation of IP and EA then also dominates  $\omega$  and leads to the general categorization of anionic radicals as weak electrophiles/strong nucleophiles. Conversely, cationic radicals are thus generally computed to be highly electrophilic, although not relating to the reactivity of the center of localized spin density but rather mostly due to the conceptual definition of  $\omega$ . In comparative studies, ionic radicals thus always held record places on both ends of the electrophilicity scale.<sup>1</sup> This appears not to be questioned so far since a strongly nucleophilic character is intuitively attributed to an anionic radical anyways, and cationic radicals are considered to be strong electrophiles, respectively. Accordingly, applying the conventional calculation method to the (di)anions **1-5** resulted in  $\omega$  values indicating strongly nucleophilic character and did not reflect the observed trends in their reaction behavior (see Table S1). In order to circumvent the dominant energy contribution from the ion's charge on both IP and EA, and to simultaneously also avoid substantial influence on the chemical character of the radical binding site, ions **1-5** were artificially “neutralized” in our calculations by the inclusion of counterions (see main manuscript).

Table S1. cDFT descriptors of ions **1-5**, **Q**, and **B**, rounded to two digits.

Ion	global $\omega$ (eV)	local $\omega^x$ (e•eV)	global $\omega^-$ (eV)	local $\omega^{-x}$ (e•eV)
<b>1</b>	0.06	0.01	8.72	1.92
<b>2</b>	0.00	0.00	7.13	2.17
<b>3</b>	0.49	0.06	5.75	1.32
<b>4</b>	1.45	0.26	5.24	-0.26
<b>5</b>	0.00	0.00	7.96	0.04
<b>Q</b>	1.49	0.53	2.41	0.65
<b>B</b>	0.04	0.02	6.44	1.53

S9 Mass spectrum measured after ion-molecule reactions of ions **1** and **2** with  $\text{CCl}_4$

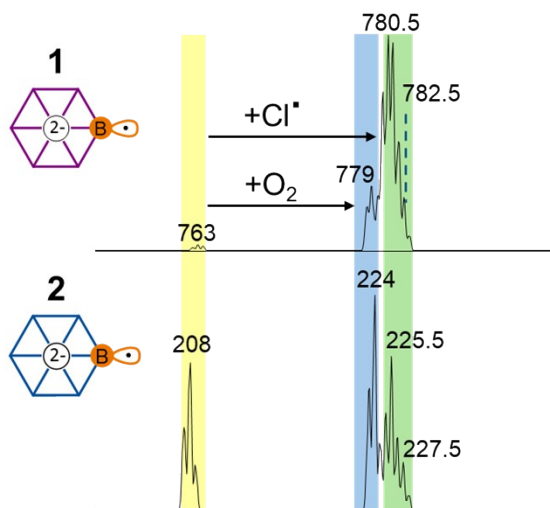


Figure S9: Mass spectra obtained after 1000 ms reaction time between isolated ions Q, **B**, **4** and **3** with carbon tetrachloride in the ion trap of a linear quadrupole ion trap mass spectrometer. The ion trap also contained ubiquitous residual  $\text{O}_2$  gas. The signal of the isolated radical ion is marked yellow. Ions **1** and **2** react with carbon tetrachloride to form the Cl atom abstraction product ions (marked in green). Binding with residual  $\text{O}_2$  gas is marked in blue.

**S10 Relative abundances of the reactant and product ions as a function of time for the reactions of ions Q, B and 1-5 with allyl iodide**

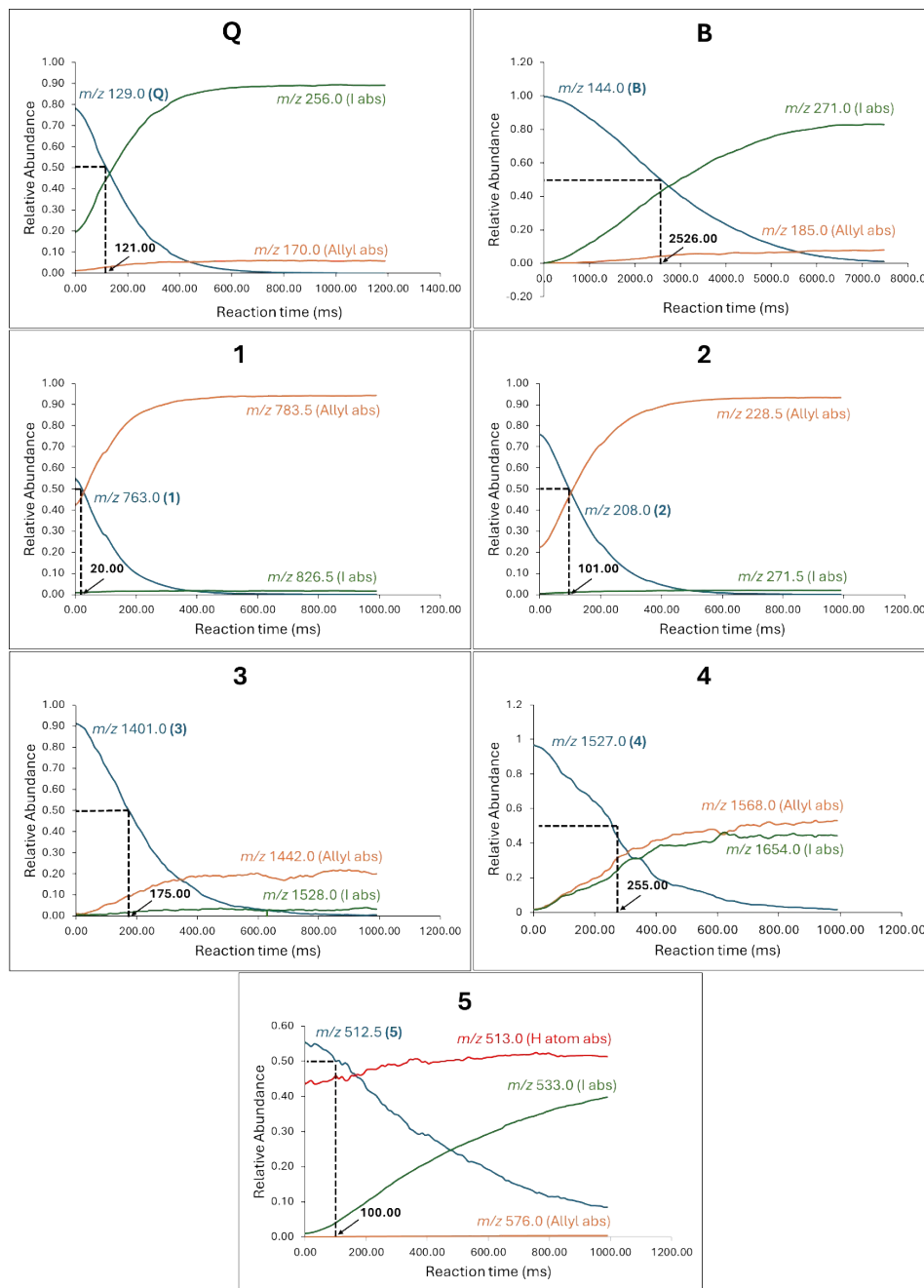


Figure S10: The relative abundances of the reactant and product ions are shown as a function of time for the reactions of ions **Q**, **B** and **1-5** with allyl iodide (nominal pressure  $0.84 \times 10^{-5}$  Torr). The time  $t_{1/2}$  is marked with a black dotted line in the diagram and shows the reaction time at which the abundance of the isolated radical ion and the sum abundance of its products each account for 50% of the total ion abundance. Note that  $1/t_{1/2}$  is proportional to the rate constant, assuming pseudo-first order kinetics. The time at which the relative abundance of the precursor ion has decreased to 50% of the total ion abundance

is marked with a dotted black line. The flux of the neutral reagent varies slightly over the course of all experiments and the measured kinetics should be interpreted qualitatively.

### S11 Mass spectrum measured after ion-molecule reactions of ion 5 with allyl iodide

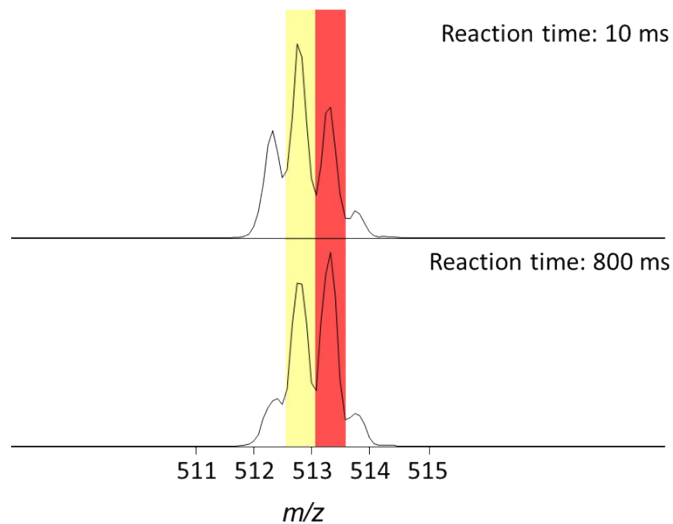


Figure S11: Section of ion-molecule reaction mass spectra obtained after isolation of the ion **5** in an ion trap containing allyl iodide introduced in the ion trap of a linear quadrupole ion trap mass spectrometer for 10 ms (top) and 800 ms (bottom) reaction time. The signal of the isolated radical ion is marked yellow, and the H atom abstraction product is marked in red.

S12 Mass spectrum measured after ion-molecule reactions with allyl chloride

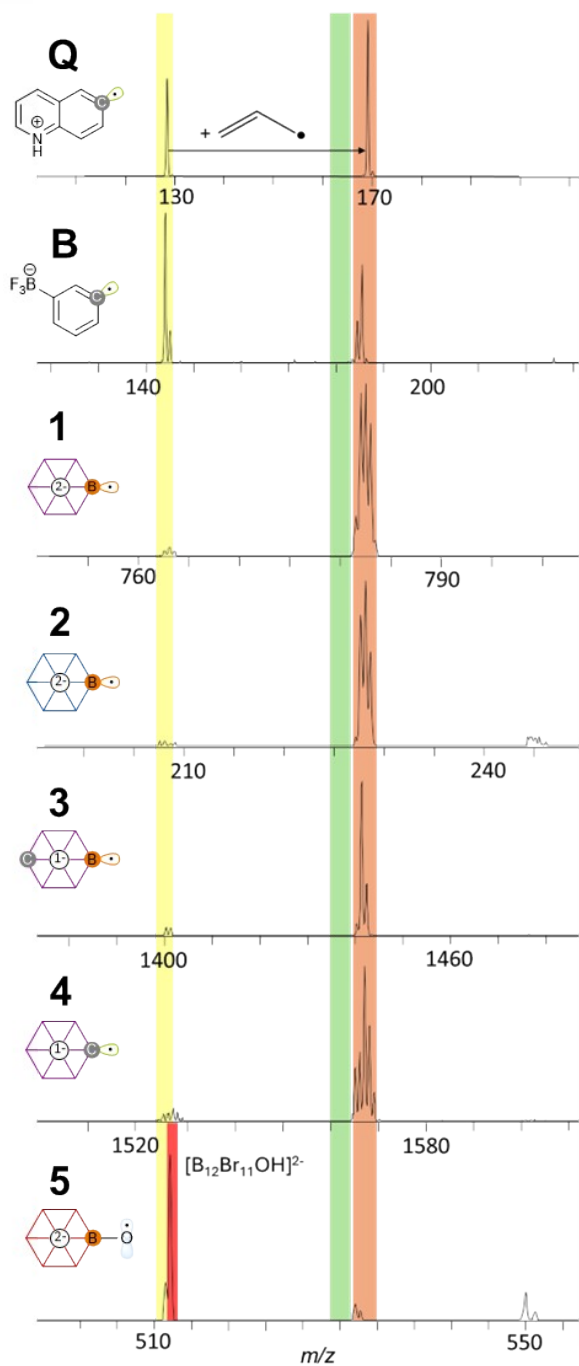


Figure S12: Mass spectra obtained after isolation of the ions **Q**, **B** and **1-5** in an ion trap containing allyl chloride introduced in the ion trap of a linear quadrupole ion trap mass spectrometer. The signal of the isolated radical ion is marked yellow. The signal of the product formed upon abstraction of allyl radical is marked orange. The Clatom abstraction product ions (marked in green) were not observed for any of these ions. In the case of ion **5**, H atom abstraction occurs as the major reaction pathway and the product signal is marked in red.

S13 PES comparison between borane radicals and phenyl/quinoline radicals

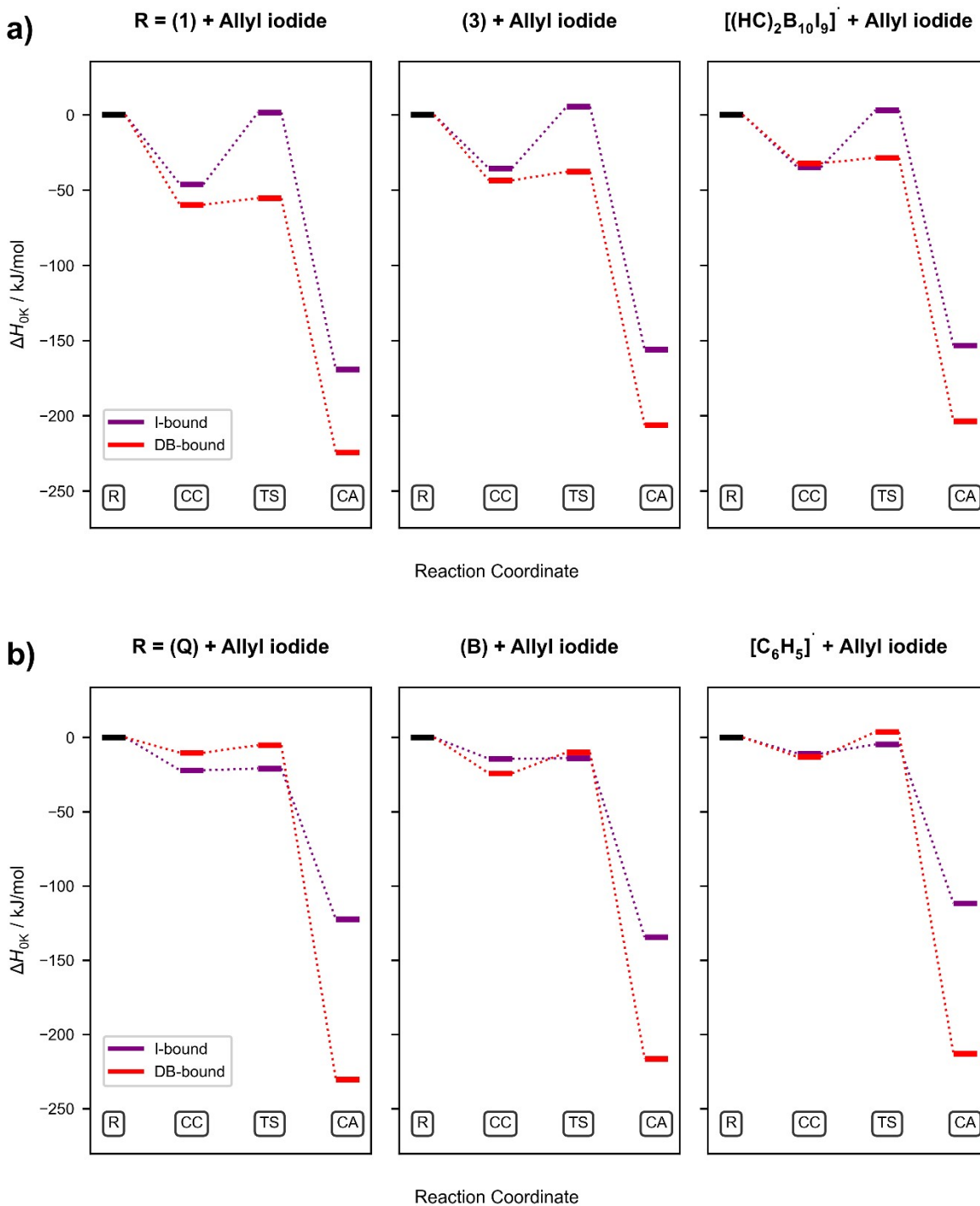


Figure S13: PES diagrams (M062X-D3/def2-TZVPP) calculated for binding of a) **1**, **3** and  $[(\text{HC})_2\text{B}_{10}\text{I}_9]^{\cdot}$  and b) **Q**, **B** and  $[\text{C}_6\text{H}_5]^{\cdot}$  to allyl iodide via its I atom (purple paths) and the C=C double bond (red paths).

**S14 PES for the reaction of allyl iodide with the hypothetical derivative  $[\text{HCB}_{11}\text{F}_{10}]^{\bullet}$**

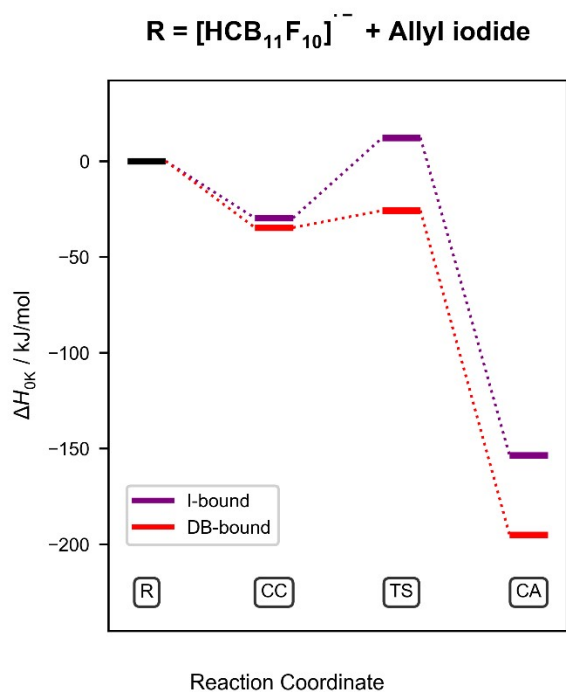


Figure S14: PES diagram (M062X-D3/def2-TZVPP) calculated for binding of  $[\text{HCB}_{11}\text{F}_{10}]^{\bullet}$  to allyl iodide via its I atom (purple path) and the C=C double bond (red path).

**S15 Calculated geometries of CC(I), TS(I) and CA(I) for ions 1 and Q**

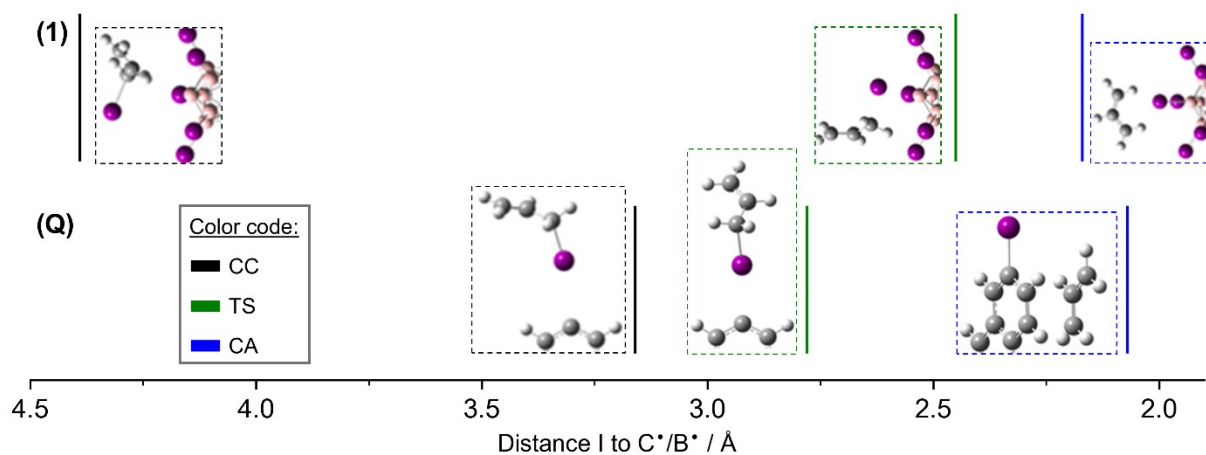


Figure S15: Excerpts of the optimized geometries of the reactant collision complexes CC (black), TSs (green), and CAs (blue) for binding of ions **1**, and **Q** to allyl iodide via its I atom, plotted against the distance of the I atom of allyl iodide to the spin-carrying C/B atoms of the ions.

## S16 Energy decomposition analysis of TS(DB) for ions **3**, **4** and **B**

Table S2: EDA results for TS(DB) for the allyl abstraction reaction between ions **3**, **4** and **B** and allyl iodide. All energy terms in kJ/mol. The major difference that leads to a lesser stabilized TS(DB) for **B** as compared to the borane-based ions **3** and **4** is the electrostatic interaction  $\Delta E_{\text{els}}$  (column marked in grey).

Ion	$\Delta E_{\text{int}}$	$\Delta E_{\text{els}}$	$\Delta E_{\text{Pauli}}$	$\Delta E_{\text{orb}}$	$\Delta E_{\text{dc}}$
<b>3</b>	-40.7	-164.6	177.5	-49.4	-4.2
<b>4</b>	-47.8	-155.4	170.4	-58.4	-4.4
<b>B</b>	-15.0	-116.0	158.5	-56.0	-1.5

## S17 References

(1) Garwood, J. J. A.; Chen, A. D.; Nagib, D. A. Radical Polarity. *J. Am. Chem. Soc.* **2024**, jacs.4c06774. <https://doi.org/10.1021/jacs.4c06774>.